Journal of Alloys and Compounds 509 (2011) 3566–3575

Contents lists available at ScienceDirect

Journal of Alloys and Compounds

journal homepage: www.elsevier.com/locate/jallcom

Structural investigation and simulation of acoustic properties of some tellurite glasses using artificial intelligence technique

M.S. Gaafar[a,d,*], Mostafa A.M. Abdeen[b], S.Y. Marzouk[c]

[a] Ultrasonic Department, National Institute for Standards, Giza, Egypt
[b] Dept. of Eng. Math. & Physics, Faculty of Eng., Cairo University, Giza, Egypt
[c] Arab Academy of Science and Technology, Al-Horria, Heliopolis, Cairo, Egypt
[d] Physics Department, Faculty of Science, Majmaah University, Zulfi, Saudi Arabia

ARTICLE INFO

Article history:
Received 4 August 2010
Received in revised form 9 December 2010
Accepted 9 December 2010
Available online 16 December 2010

Keywords:
Tellurite glasses
Ultrasonic velocities
Elastic moduli
Artificial intelligence

ABSTRACT

The developments in the field of industry raise the need for simulating the acoustic properties of glass materials before melting raw material oxides. In this paper, we are trying to simulate the acoustic properties of some tellurite glasses using one of the artificial intelligence techniques (artificial neural network). The artificial neural network (ANN) technique is introduced in the current study to simulate and predict important parameters such as density, longitudinal and shear ultrasonic velocities and elastic moduli (longitudinal and shear moduli). The ANN results were found to be in successful good agreement with those experimentally measured parameters. Then the presented ANN model is used to predict the acoustic properties of some new tellurite glasses. For this purpose, four glass systems xNb$_2$O$_5$–$(1-x)$TeO$_2$, 0.1PbO–xNb$_2$O$_5$–$(0.9-x)$TeO$_2$, 0.2PbO–xNb$_2$O$_5$–$(0.8-x)$TeO$_2$ and 0.05Bi$_2$O$_3$–xNb$_2$O$_5$–$(0.95-x)$TeO$_2$ were prepared using melt quenching technique. The results of ultrasonic velocities and elastic moduli showed that the addition of Nb$_2$O$_5$ as a network modifier provides oxygen ions to change [TeO$_4$] tbps into [TeO$_3$] tps.

1. Introduction

Over the last few decades, tellurite-based glasses have been the subject of both academic and technological interest. These glasses possess high refractive indices with low dispersion values, a low tendency to crystallize, good chemical resistance, good semiconducting properties and low melting points [1–6]. The structure of tellurite glasses has been investigated previously using IR, Raman spectroscopy, X-ray, and neutron diffraction techniques. The main focus of these studies was on the structural units in the glass network. In general, the structure and properties of oxide glasses are strongly dependent on the nature and concentration of the constituent oxides. Thus, in tellurite glasses, modifier atoms cause changes in the basic structural units, namely TeO$_4$ trigonal bipyramid (tbp) and TeO$_3$ trigonal pyramid (tp) units, both of which have a lone pair of electrons occupying one of the equatorial positions.

Niobium-containing tellurite glass with starting composition of $(90-x)$TeO$_2$–10Nb$_2$O$_5$–(x)ZnO (x = 0–15 mol%) have been prepared by Mohamed et al. [7] using melt-quenching method and studied the effect of reduction of TeO$_2$ with simultaneous increase in ZnO on elastic properties. Infrared (IR) absorption spectra showed increase in intensity of NbO$_6$-assigned peak accompanied by increase in intensity of ZnO$_4$ tetrahedra and TeO$_4$ trigonal bipyramid (tbp) assigned peaks indicating formation of both non-bridging oxygen, NBO and bridging oxygen, BO, respectively, with addition of ZnO. The initial drop in ultrasonic velocity and related elastic moduli observed at x = 5 mol% indicates weakening of network rigidity of the glass system due to structural modification as a direct effect of TeO$_2$ reduction and existence of NBO. However, further replacement of TeO$_2$ by ZnO at x > 5 mol% contributed to increase in BO causing rigidity of the glass network to improve.

The physical and optical properties (density, refractive index, molar volume, glass temperature transition (T_g), crystallization temperature (T_x), optical absorption and energy gap) were determined by Wang et al. [8] for the ternary TeO$_2$–Nb$_2$O$_5$–Bi$_2$O$_3$ glass system. The glasses have high refractive indexes, which are more than 2.0. It was found that the addition of Nb$_2$O$_5$ and Bi$_2$O$_3$ to TeO$_2$ glass increases the refractive index value as well as density, whereas the TeO$_2$–Nb$_2$O$_5$–Bi$_2$O$_3$ glass system has small domain. The refractive index of the glasses increases with increasing molar volume, tendency for small energy band gap, optical band gap and metallization criterion.

Tellurite glasses containing calcium and bismuth oxides have been prepared by Chagraoui et al. [9] at 800 °C and investigated

* Corresponding author. Tel.: +20 23867454; fax: +20 23867451.
E-mail addresses: mohamed_s_gaafar@hotmail.com (M.S. Gaafar), mostafa_a_m_abdeen@hotmail.com (M.A.M. Abdeen), samir_marzouk2001@yahoo.com (S.Y. Marzouk).

0925-8388/$ – see front matter © 2010 Elsevier B.V. All rights reserved.
doi:10.1016/j.jallcom.2010.12.064

by X-ray diffraction, DSC, IR and Raman spectroscopy. The crystalline phases of glasses in TeO_2–CaO revealed γTeO_2 phase which transforms into the stable αTeO2 phase up to 500 °C. IR and Raman studies show the transition of TeO_4, TeO_{3+1} and TeO_3 units with increasing CaO content. The value of refractive index and density of glasses have been measured. The investigation in the system using XRD reveals new phases.

Zou and Toratani [10] have modified the derived equations by Makishima and Machenzie for direct determination of the elastic modulus of glasses from composition and obtained an excellent agreement between the measured and estimated values of elastic modulus for over 50 different glasses. The authors used these derived equations to develop a new glass Li_2O–MgO–Al_2O_3–Y_2O_3–TiO_2–SiO_2 system with high elastic modulus to provide a solution to the vibration problem rapid rotation magnetic disk and allow higher track density per inch to be achieved for high performance hard-disk drives (HDDs).

Artificial intelligence had proved its capability in simulating and predicting the behavior of the different physical phenomena in most of the engineering fields. artificial neural network (ANN) is one of the artificial intelligence techniques that have been incorporated in various scientific disciplines. Kheireldin [11] presented a study to model the hydraulic characteristics of severe contractions in open channels using ANN technique. The successful results of his study showed the applicability of using the ANN approach in determining the relationship between different parameters with multiple input/output problems. Abdeen [12] developed neural network model for predicting flow characteristics in irregular open channels. The developed model proved that ANN technique was capable with small computational effort and high accuracy of predicting flow depths and average flow velocities along the channel reach when the geometrical properties of the channel cross sections were measured or vice versa. Allam [13] used the artificial intelligence technique to predict the effect of tunnel construction on nearby buildings, which is the main factor in choosing the tunnel route. Allam [13] predicted the maximum and minimum differential settlement necessary precautionary measures. Abdeen [14] presented a study for the development of ANN models to simulate flow behavior in open channel infested by submerged aquatic weeds. Mohamed [15] proposed an artificial neural network for the selection of optimal lateral load-resisting system for multi-story steel frames. Mohamed [15] proposed the neural network to reduce the computing time consumed in the design iterations. Abdeen [16] utilized ANN technique for the development of various models to simulate the impacts of different submerged weeds' densities, different flow discharges and different distributaries operation scheduling on the water surface profile in an experimental main open channel that supplies water to different distributaries. Abdeen and Hodhod [17] introduced the (ANN) technique to investigate the effect of light local weight aggregate on the performance of the produced light weight concrete. The results of their study showed that the ANN method with less effort was very efficiently capable of simulating the effect of different aggregate materials on the performance of light weight concrete.

In the present work, four different glass series xNb_2O_5–$(1-x)TeO_2$, $0.1PbO$–xNb_2O_5–$(0.9-x)TeO_2$, $0.2PbO$–xNb_2O_5–$(0.8-x)TeO_2$ and $0.05Bi_2O_3$–xNb_2O_5–$(0.95-x)TeO_2$ with different Nb_2O_5 and constant PbO and Bi_2O_3 contents were investigated. Both ultrasonic velocities and elastic moduli were determined to investigate the effect of incorporation of Nb_2O_5 on the network structure of these glasses. Then, a model using one of the artificial intelligence techniques (ANN) was designed in order to predict both the ultrasonic velocities and elastic moduli of these four different glass series. Such a model enables the direct simulation of very important parameters such as density, both ultrasonic velocities (longitudinal & shear) and elastic moduli without melting raw material oxides as in some cases, they are of high costs.

Table 1
Glass compositions.

Glass composition (mol%)			
TeO_2	Bi_2O_3	Nb_2O_5	PbO
0.95	–	0.05	–
0.9	–	0.1	–
0.85	–	0.15	–
0.8	–	0.2	–
0.9	–	0	0.1
0.7	–	0.2	0.1
0.8	–	0	0.2
0.7	–	0.1	0.2
0.6	–	0.2	0.2
0.75	0.05	0.2	–
0.7	0.05	0.25	–

2. Experimental details

2.1. Preparation of glasses

Four glass series xNb_2O_5–$(1-x)TeO_2$, $0.1PbO$–xNb_2O_5–$(0.9-x)TeO_2$, $0.2PbO$–xNb_2O_5–$(0.8-x)TeO_2$ and $0.05Bi_2O_3$–xNb_2O_5–$(0.95-x)TeO_2$ with different Nb_2O_5 and constant PbO and Bi_2O_3 contents have been prepared by rapid quenching method. Batches of each glass composition are listed in Table 1. The analytical grade materials of purity more than 99.9% of TeO_2, Nb_2O_5, PbO, and Bi_2O_3 chemicals were used to prepare the glass samples.

Appropriate amounts in wt% of chemicals in powder form were weighed using a digital balance (HR–200) having sensitivity of ±0.0001 gm. The homogeneity of the chemicals mixture was achieved by repeated grinding using an agate mortar. The mixture was preheated at 673 K for 60 min (in a covered platinum crucible to prevent volatilization of TeO_2) to remove H_2O and CO_2. The preheated mixture was then melted in a muffle furnace whose temperature was controlled at 1173 K for 60 min, and bubble free liquid was obtained. The mixture was stirred intermediately in order to obtain homogeneous mixture. The molten mixture was then poured in a cuboidal-shaped split mold made of mild steel which had been preheated at about 575 K. Annealing was carried out for a period of 60 min at 723 K. Bulk glass samples of about $1 \times 1 \times 4\ cm^3$ were therefore obtained.

In order to measure the ultrasonic velocity accurately, each glass sample was first ground on a glass plate using SiC abrasives by setting it in a holder to maintain the two opposite faces parallel. It was then polished with fine alumina abrasive and machine oil on a glass plate. The variation in the sample thickness was found to be ±20 μm. The amorphous nature in all glass samples was confirmed using X-ray diffraction (XRD).

2.2. Density measurements

Density (ρ) of all glass samples was calculated employing Archimedes principle using toluene as buoyant and applying the relation;

$$\rho = \rho_b \left(\frac{W_a}{W_a - W_b} \right) \quad (1)$$

where ρ_b is the density of the buoyant, W_a and W_b are the sample weights in air and the buoyant respectively. The experiment was repeated three times, and the error in density measurement in all glass samples is $\pm 0.005\ g/cm^3$.

2.3. Ultrasonic velocity measurements

The ultrasonic wave velocities were obtained applying pulse–echo technique by measuring the elapsed time between the initiation and the receipt of the pulse appearing on the screen of a flaw detector (USIP20–Kraütkramer) by standard electronic circuit (Hewlett Packard 54615 B). The velocity was therefore, calculated by dividing the round trip distance by the elapsed time according to the relation;

$$U = \frac{2X}{\Delta t} \quad (2)$$

where X is the sample thickness and Δt is the time interval.

All velocity measurements in this study were carried out at 4 MHz frequency, and at room temperature 298 K. The estimated error in velocity measurements was ±20 m/s for longitudinal wave velocity (U_ℓ) and ±12 m/s for shear wave velocity (U_s).

2.4. Determination of elastic moduli

Elastic moduli (longitudinal (L), shear (G), bulk (K), and Young's (E)) as well as Debye temperature (θ_D), and Poisson's ratio (σ) of the glasses series have been determined from the measured ultrasonic wave velocities and density using the relations [18];

$$\begin{aligned} L &= \rho U_\ell^2 \\ G &= \rho U_s^2 \\ K &= L - \left(\frac{4G}{3}\right) \\ E &= (1+\sigma)2G \\ \sigma &= \left(\frac{(L-2G)}{2(L-G)}\right) \end{aligned} \tag{3}$$

$$\theta_D = \left(\frac{h}{k_B}\right)\left(\frac{3\psi N_A}{4\pi V_a}\right)^{1/3} U_m \tag{4}$$

where h is Planck's constant, k_B is Boltzmann's constant, N_A is Avogadro's number, V_a is the molar volume calculated from the effective molecular weight and density (i.e. M/ρ), Ψ is the number of atoms in the chemical formula, and U_m is the mean ultrasonic velocity defined by the relation,

$$U_m = \left(\frac{1}{3}\left(\frac{1}{U_\ell^3} + \frac{2}{U_s^3}\right)\right)^{-1/3} \tag{5}$$

3. Theoretical models

3.1. Bond compression model

The structure of oxide glasses can be described in terms of bond compression model which was first introduced by Bridge et al. [19] for the study of single-component glass which was later developed for multi-component glasses [20]. The model assumed two assumptions:

(i) The elastic moduli only depends on the "connectivity" of the network (number of bonds per cation) and on the average force constant. The calculated bulk modulus (K_{bc}) according to this model and the first-order stretching-force constant f, can be estimated according to the relations;

$$\begin{aligned} K_{bc}(\text{GPa}) &= \frac{\rho N_A}{9M}\sum_i^n x_i(n_f) r_i^2 f_i \\ f_i &= \frac{1.7}{r_i^3} \end{aligned} \tag{6}$$

where x_i is the mole fraction of the i^{th} oxide, n_f is the number of network bonds per glass formula unit and r_i is the bond length. Accordingly, the average bond stretching-force constant $\overline{F}$ for a three-dimensional poly-component oxide glasses can be estimated [20].

(ii) The ratio between the calculated bulk moduli and the experimental one (K_{bc}/K_{exp}) is assumed to be directly proportional to the atomic ring size (ℓ). The atomic ring size is defined as the ring perimeter (number of bonds times bond length divided by π) and is given by the relation;

$$\ell(\text{nm}) = \left[0.0106\frac{F_b}{K_{exp}}\right]^{0.26} \tag{7}$$

where K_{exp} is the experimental bulk modulus and Fb is the bond bending force constant of the glass, which is proportional to the average bond stretching force constant $\overline{F}$.

The average crosslink density per unit formula of glass is given as,

$$\overline{n_c} = \frac{1}{\eta}\sum_i x_i(n_c)_i(N_c)_i \tag{8}$$

where n_c is the number of crosslink density per cation which equals the number of bonds less 2, N_c is the number of cations per glass formula unit and η is the total number of cations per glass formula unit.

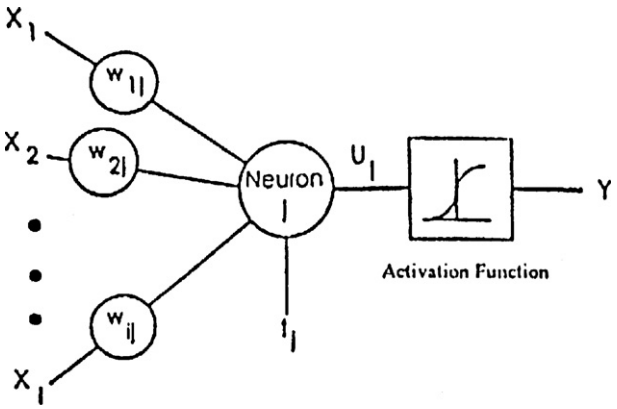

Fig. 1. Typical picture of a model neuron that exists in every neural network.

Also, the average number of bonds per unit volume of glass is given as,

$$\begin{aligned} n_b &= n_f N_f \\ &= nN_A\rho/M \end{aligned} \tag{9}$$

where N_f is the number of formula units per unit volume and n is the co-ordination number.

3.2. Makishima and Mackenzie model

Makishima and Mackenzie [21,22] presented theoretical model to calculate the elastic moduli of oxide glasses in terms of chemical composition, which depends only on packing density (V_t) and dissociation energy (G_t) of the oxide constituents. The elastic moduli and Poisson's ratio were given as follows:

$$\begin{aligned} E_m &= 2V_tG_t \\ K_m &= \beta V_t E_m \\ G_m &= \frac{3E_mK_m}{9K_m - E_m} \\ \sigma_m &= \frac{E_m}{2G_m} - 1 \end{aligned} \tag{10}$$

where β is the slope deduced from the linear regression between the experimentally obtained bulk modulus and the product of the packing density multiplied by the experimentally obtained Young's modulus.

3.3. Numerical model

It is quite important within the current study to highlight the advantages and limitations of the artificial neural network (ANN). ANN technique can simulate and predict very important parameters such as density, both ultrasonic velocities (longitudinal & shear) and elastic moduli without the need to go through an experimental program which will save money and time. On the other hand, ANN is limited to the existence of part of data availability for developing and training the network and is sensitive to the accuracy of the data which is quite reflected in the predicted results. This means that if the training data are not accurate enough, the predicted results will not be accurate because of data accuracy.

Neural networks are models of biological neural structures. Abdeen [12] has described in details, the structure of any neural network. Briefly, the starting point for most networks is the model neuron as shown in Fig. 1. This neuron is connected to multiple inputs and produces single output. Each input is modified by a weighting value (w). The neuron will combine these weighted

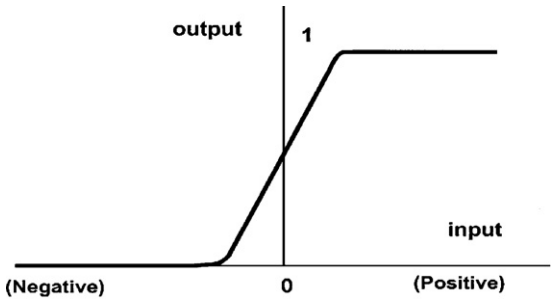

Fig. 2. The sigmoid activation function.

inputs with reference to a threshold value and an activation function to determine its output. This behavior follows closely the real neurons work of the human's brain. In the network structure, the input layer is considered as distributor of the signals from the external world while hidden layers which are considered to be feature detectors of such signals. On the other hand, the output layer is considered as a collector of the features detected and produces the response.

3.4. Neural network operation

It is quite important for the reader to understand how the neural network operates to simulate different physical problems. The output of each neuron is a function of its inputs (X_i). In more details, the output (Y_j) of the j^{th} neuron in any layer is described by two sets of equations as follows:

$$U_j = \sum \left(X_i w_{ij}\right) \tag{11}$$

and

$$Y_j = F_{th}\left(U_j + t_j\right) \tag{12}$$

For every neuron, j, in a layer, each of the i inputs, X_i, to that layer is multiplied by the previously established weight, w_{ij}. These are all summed together, resulting in the internal value of this operation, U_j. This value is then biased by the previously established threshold value, t_j, and sent through an activation function, F_{th}. This activation function can takes several forms such as; Step, Linear, Sigmoid, Hyperbolic, and Gaussian functions. The Hyperbolic function used in this study, is shaped exactly as the Sigmoid one with the same mathematical representation as in Eq. (12), but it ranges from −1 to +1 rather than from 0 to 1 as in the Sigmoid one (Fig. 2). Thus it has the interesting property, that there is inhibition near 0, but values at either extreme will be excited to the full level in opposite sense. In addition, the Hyperbolic function can be considered as a switch with an intermediate range where it can be discriminated. However the Linear function always generates outputs which are proportional to the inputs up to the level of full output. An important distinction is that the linear function is stepped at the point when it transforms from proportional output to the full output, whereas the Hyperbolic and Sigmoid functions are always smooth and are differentiable. Differentiability of the neuron activation function is an important factor in getting consistent back-propagation training behavior, Shin [23].

$$f(x) = \frac{1}{1+e^{-x}} \tag{13}$$

Table 3
Key output variables for ANN model.

Output variables				
Density	Longitudinal velocity (U_l)	Shear velocity (U_S)	Longitudinal modulus (L)	Shear modulus (G)

The resulting output, Y_j, is an input to the next layer or, it is a response of the neural network if it is the last layer. In applying the neural network technique, in this study Neuralyst Software was used by Shin [23].

3.5. Neural network training

The next step in neural network procedure is the training operation. The main purpose of this operation is to tune up the network to what it should be produced as a response. From the difference between the desired response and the actual response, the error is determined and a portion of it is back propagated through the network. At each neuron in the network, the error is used to adjust the weights and the threshold value of this neuron. Consequently, the error in the network will be less for the same inputs at the next iteration. This corrective procedure is applied continuously and repetitively for each set of inputs and corresponding set of outputs. This procedure will decrease the individual or total error in the responses to reach a desired tolerance.

Once the network reduces the total error to the satisfactory limit, the training process may stop. The error propagation in the network starts at the output layer with the following equations:

$$w_{ij} = w'_{ij} + LR\left(e_j X_i\right) \tag{14}$$

And

$$e_j = Y_j\left(1 - Y_j\right)\left(d_j - Y_j\right) \tag{15}$$

where, w_{ij} is the corrected weight, w'_{ij} is the previous weight value, LR is the learning rate, e_j is the error term, X_i is the i^{th} input value, Y_j is the output and d_j is the desired output.

3.6. Artificial neural network model

To simulate and predict the acoustic properties of some tellurite glasses such as density, (longitudinal and shear) ultrasonic velocities and elastic moduli (Longitudinal and shear), numerical model was using artificial neural network technique was designed to simulate these important parameters. To develop a neural network model, first input and output variables have to be determined. Input variables are chosen according to the nature of the problem and the type of data that would be collected. To clearly specify the key input variables and their associated outputs, Tables 2–3 are designed to summarize the neural network key input and output variables, respectively.

Several neural network architectures are designed and tested in this study to finally determine the best network model to simulate very accurately the acoustic properties of tellurite glasses based on minimizing the root mean square error (RMS-error). Fig. 3 shows a schematic diagram for a generic neural network.

The training procedure for the developed ANN model, in the current study, uses the experimental acoustic properties of some tellurite glasses and then the model will be able to predict the

Table 2
Key input variables for ANN model.

Input variables															
BaO	Sm_2O_3	PbO	Nb_2O_5	La_2O_3	V_2O_5	Bi_2O_3	Li_2O	B_2O_3	CuO	CeO_2	K_2O	WO_3	TeO_2	Molecular weight	Density (calculated)

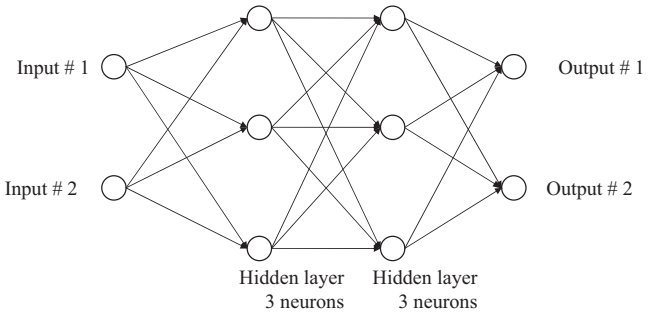

Fig. 3. General schematic diagram of a simple generic neural network.

properties of other tellurite glasses without need to make new experiments.

Table 4 shows the final neural network model and its associate number of neurons. The input and output layers represent the key input and output variables described previously.

The parameters of the network model developed in the current study can be described with their tasks as follows:

Learning rate (*LR*): determines the magnitude of the correction term applied to adjust each neuron's weights during training process = 1.

Momentum (M): determines the "life time" of the correction term as the training process takes place = 0.9.

Training tolerance (TRT): defines the percentage error allowed in comparing the neural network output to the target value to be scored as "right" during the training process = 0.001

Testing tolerance (TST): it is similar to training tolerance, but it is applied to the neural network outputs and the target values only for the test data = 0.003

Input noise (IN): provides a slight random variation to each input value for every training epoch = 0.

Function gain (FG): allows a change in the scaling or width of the selected function = 1.

Scaling margin (SM): adds additional headroom, as a percentage of range, to the rescaling computations used by Neuralyst Software, Shin (1994), in preparing data for the neural network or interpreting data from the neural network = 0.1.

Training epochs: number of trails to achieve the present accuracy = 231940

Percentage relative error (PRR): percentage relative error between the numerical results and actual measured value for and is computed according to equation (16) as follows:

$$\mathrm{PRE} = \left(\frac{\text{Absolute Value (ANN\_PR-AMV)}}{\text{AMV}}\right) \times 100 \qquad (16)$$

where:

ANN_PR: predicted results using the developed ANN model.

AMV: actual measured value.

MPRE: maximum percentage relative error during the model results for the training step = 0.5%.

Table 4
The developed neural network model.

No. of layers	No. of neurons in each layer				
	Input layer	First hidden	Second hidden	Third hidden	Output layer
5	16	13	9	7	5

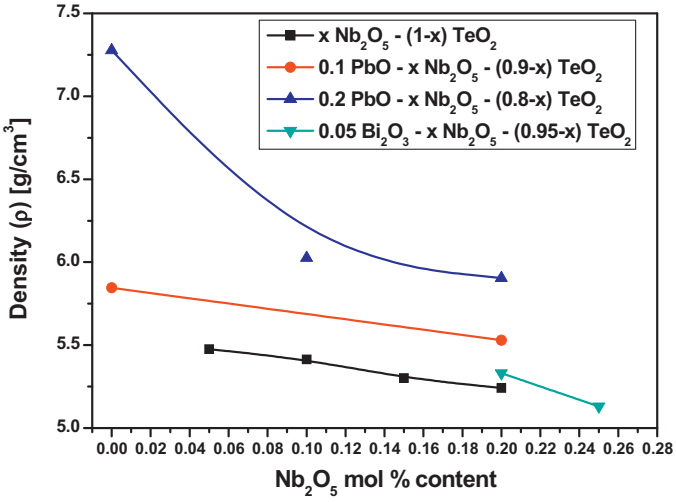

Fig. 4. Variation of density of the four investigated glass series with Nb_2O_5 mol% content.

4. Results and discussions

4.1. Density and molar volume

Density is a powerful tool for exploring changes in the structure of glasses. It is affected by structural softening/compactness, change in geometrical configuration, coordination number, cross-link density and dimension of interstitial spaces of the glass.

The chemical composition of studied glasses, their density values and molar volume are given in Table 5 while Fig. 4 showed the variation of density with addition of different Nb_2O_5 mol% contents at the expense of TeO_2 while the contents of PbO and Bi_2O_3 contents are constants. It is evident that with increasing Nb_2O_5 mol% content, the density values were found to decrease. The decrease in density values with addition of Nb_2O_5 is expected if we take into consideration the additive density rule. The density of Nb_2O_5 is 4.600 g/cm^3 which is much lower than TeO_2 (5.900 g/cm^3), Bi_2O_3 (8.900 g/cm^3) and PbO (9.350 g/cm^3) [24]. As suggested by Komatsu et al. [25], the structural unit of TeO_2-based glasses changes gradually from asymmetrical TeO_4 trigonal bipyramid (tbps) to TeO_3 trigonal pyramid (tps) accompanied with increasing amounts of other components such as alkali and alkali earth elements.

At the same time, the values of molar volume (V_a) were found to increase with increasing Nb_2O_5 contents as shown in Fig. 5. This increase was expected since the atomic radii of tellurium, niobium, bismuth and lead atoms are 1.38 Å, 1.64 Å, 1.48 Å and 1.46 Å, respectively. In general, the increase in molar volume indicates the increase of voids in the glass network structure. Therefore, the increase in molar volume with increasing modifier Nb_2O_5 content confirms the transformation of TeO_4 trigonal bipyramids to TeO_3 trigonal pyramids with non-bridging oxygen atoms and consequently means that the structure becomes more open. These behaviors were confirmed by the results of fractal bond connectivity ($d = 4G/K$) and number of bonds per unit volume which were calculated according to bond compression model [19,20] as shown in Table 5.

4.2. Ultrasonic studies

As shown in Eq. (3), the elastic moduli are proportional to the square of velocity and a plot of ultrasound velocities vs composition is indicative of relative structure. The compositional dependence of U_l and U_s are shown in Table 5 shows the variation of longitudinal, shear, bulk and Young's elastic moduli as a function of Nb_2O_5

Table 5
Density (ρ), molar volume (V_a), longitudinal velocity (U_l), shear velocity (U_s), bulk modulus (K), Poisson's ratio (σ), Debye temperature (θ_D), fractal bond connectivity (d), Dissociation energy (G_i), cross-link density (n_c), number of bonds per unit volume (n_b) and micro-hardness (H).

Glass composition (mol%)				ρ (g/cm^3)	V_a x10^{-6} (m^3/mol)	U_l (m/s)	U_s (m/s)	K (GPa)	σ	θ_D (K)	d	G_i (kJ/cm^3)	n_c	n_b x10^{25} (m^{-3})	H (GPa)
TeO_2	Bi_2O_3	Nb_2O_5	PbO												
0.95		0.05		5.475	30.12	3352	1876	35.83	0.272	249	2.151	50.86	2.10	8.197	2.929
0.9		0.1		5.414	31.44	3464	1911	38.60	0.281	255	2.049	51.81	2.20	8.045	2.883
0.85		0.15		5.302	33.11	3677	1949	44.83	0.305	261	1.797	52.77	2.30	7.822	2.623
0.8		0.2		5.242	34.50	3922	2087	50.19	0.302	281	1.820	53.72	2.40	7.681	3.006
0.9		0	0.1	5.845	28.39	3091	1746	32.09	0.266	229	2.221	47.45	2.00	8.484	2.783
0.7		0.2	0.1	5.529	33.86	3767	2079	46.59	0.281	287	2.052	51.26	2.42	7.826	3.489
0.8		0	0.2	7.278	23.68	2882	1495	38.76	0.316	205	1.679	44.99	2.00	10.174	1.996
0.7		0.1	0.2	6.025	30.36	3151	1784	34.25	0.264	241	2.239	46.89	2.22	8.330	3.016
0.6		0.2	0.2	5.904	32.78	3692	2177	43.17	0.233	306	2.593	48.79	2.44	8.082	4.971
0.75	0.05	0.2		5.330	36.80	3633	1879	45.26	0.317	262	1.663	52.80	2.46	7.364	2.291
0.7	0.05	0.25		5.130	39.27	3990	2175	49.31	0.289	300	1.969	53.75	2.56	7.054	3.420

Table 6
(E/G) ratio, theoretical bond compression bulk modulus (K_{bc}), average ring diameter (ℓ), (K_{bc}/K_{exp}) ratio, theoretical Makishima and Mackenzie bulk modulus (K_m) and theoretical Makishima and Mackenzie Poisson's ratio (σ_m).

Glass composition (mol%)				(E/G)	K_{bc} (GPa)	ℓ (nm)	(K_{bc}/K_e)	K_m (GPa)	σ_m
TeO_2	Bi_2O_3	Nb_2O_5	PbO						
0.95		0.05		2.544	77.54	4.874	2.164	38.32	0.268
0.9		0.1		2.563	75.47	4.753	1.955	40.49	0.272
0.85		0.15		2.609	72.81	4.545	1.624	42.40	0.276
0.8		0.2		2.605	70.95	4.389	1.414	48.48	0.298
0.9		0	0.1	2.531	80.62	5.032	2.513	32.03	0.250
0.7		0.2	0.1	2.562	72.03	4.462	1.546	47.19	0.301
0.8		0	0.2	2.632	96.30	4.776	2.485	38.39	0.296
0.7		0.1	0.2	2.528	77.56	4.874	2.264	37.89	0.280
0.6		0.2	0.2	2.467	74.12	4.538	1.717	43.81	0.263
0.75	0.05	0.2		2.635	67.85	4.499	1.499	42.06	0.238
0.7	0.05	0.25		2.577	64.53	4.377	1.309	52.41	0.235

contents. As in Table 5, both U_l and U_s and elastic moduli increase with increase of Nb_2O_5 concentration over the entire composition studied. This variation of ultrasound wave velocities and elastic moduli can be explained on the basis of the structural consideration of tellurite glass network. As reported before by Lin et al. [26], the network structure of the TeO_2–Nb_2O_5 glasses changes with the content of Nb^{5+} ions. When the Nb_2O_5 content is lower, most of Te^{4+} ions exist as [TeO_4] tbps and form Te–O chains, the [TeO_4] tbps link each other both in apical sharing and in edge sharing, only a few of [TeO_3] tps exist in the glass network. The Nb^{5+} ions exist as [NbO_6] octahedra to link the chains as shown in Fig. 6. Due to insufficient linkage of the Te–O chains because of insufficient amount of Nb^{5+} ions in the TeO_2–Nb_2O_5 glass, the glass network easily loses its stability. Therefore, the metastable edge-sharing [TeO_4] tbps will first form edge-sharing β-TeO_2 phase at lower temperature. The apical-sharing [TeO_4] tbps are more stable than the edge-sharing ones, they will form α-TeO_2 phase with similar structure at higher temperatures. Te–O chains connected with Nb^{5+} ions are more stable, they will form $Te_3Nb_2O_{11}$ phase with apical sharing structure [27] at much higher temperatures. When the

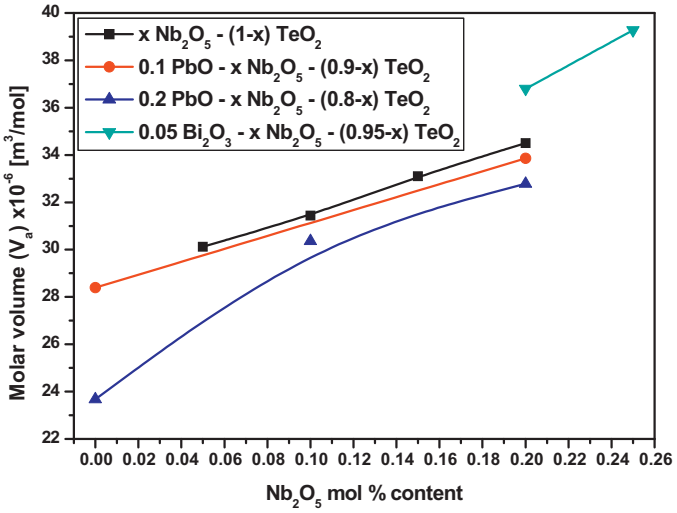

Fig. 5. Variation of molar volume of the four investigated glass series with Nb_2O_5 mol% content.

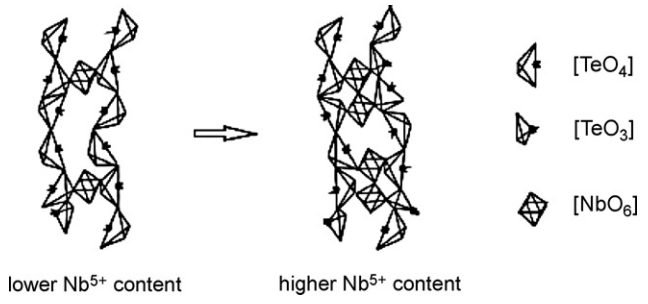

Fig. 6. Schematic diagram of the TeO_2 glass network modified by Nb_2O_5 as a network modifier.

Nb_2O_5 content in the glass is increased, more and more Nb^{5+} ions will connect Te–O chains as [NbO_6] octahedra, just like the [NbO_6] octahedral chain between [TeO_4] tbp chains in the $Nb_2Te_4O_{13}$ crystal, in which some of the polyhedra are linked by edge sharing [28]. The introduced Nb_2O_5 will also provide oxygen ions to change more [TeO_4] tbps into [TeO_3] tps. It seems that the glass network is strengthened by enhancing the linkage of Te–O chains. The tellurite network will also come to homogenization, because of uniform distribution of Nb^{5+} ions among the Te–O chains, though some of the tellurium-oxide polyhedra still link each other in edge sharing. These results were confirmed by the increase in both cross-link density (n_c) which was calculated according to bond compression model [19] and dissociation energy (Gi) which was calculated according to Makishima and Machenzie model [21,22] as shown in Table 2. Moreover, the increase in bulk modulus is may be due to the incorporation of Nb_2O_5 contents with bond energy of Nb–O bond (≈771 kJ/mol) which is higher than the bond energy of Pb–O (≈382 kJ/mol) and Te–O bonds (≈376 kJ/mol) [24]. Further more, the calculated values of bulk modulus (K_m) (see Table 6) according to Makishima and Machenzie model were found to be in good agreement with those determined experimentally in Table 5.

Poisson's ratio (σ) is formally defined for any structure as the ratio of lateral to longitudinal strain produced when tensile forces are applied. In solid materials, the tensile strain produced in the network is unaffected by the cross-links while the lateral strain is greatly decreased with increasing covalence of bonds [19]. Bridge and Higazy [20] have suggested a close correlation between Poisson's ratio and cross-link density which is defined as the number of bridging bonds per cation. They reported that crosslink density values of two, one, and zero are related to the values of Poisson's ratio of 0.15, 0.29, and 0.4, respectively. For stresses parallel to chain structure, Young's modulus (E) will increase with bond stretching force constant while shear modulus (G) will increase with the bond bending force constant. Thus, as the ratio of bond bending force constant to stretching force constant increases, the ratio (E/G) decreases [19,20].

In the first two glass systems $x$$Nb_2O_5$–$(1-x)$$TeO_2$ and 0.1PbO–$x$$Nb_2O_5$–$(0.9-x)$$TeO_2$, with increasing modifier Nb_2O_5 mol% content the values of (E/G) ratio were found to increase as shown in Table 6, which means the decrease in the ratio of bond bending force constant to stretching force constant confirming that most of Nb^{5+} ions are associated with Te^{4+} ions to change [TeO_4] tbps into [TeO_3] tps without the linking of Te–O chains. Therefore, the values of fractal bond connectivity (d) were found to decrease with increasing Nb_2O_5 mol% content. Moreover, the increase in Poisson's ratio (σ) in these two glass systems means the increase in the ratio of lateral to longitudinal strains confirming the decrease in the linkages between Te–O chains.

At the same time, in the last two glass systems, 0.2PbO–$x$$Nb_2O_5$–$(0.8-x)$ TeO_2 and 0.05Bi_2O_3–x Nb_2O_5–$(0.95-x)$$TeO_2$, with increasing Nb_2O_5 mol% content the values of (E/G) ratio were found to decrease as shown in Table 6, which consequently means the increase in the ratio of bond bending force constant to stretching force constant confirming that the Nb^{5+} ions are acted to increase the linking of Te–O chains. Therefore, the values of fractal bond connectivity (d) were found to increase with increasing Nb_2O_5 mol% content. Moreover, the decrease in Poisson's ratio (σ) in these two glass systems means the decrease in the ratio of lateral to longitudinal strains confirming the increase in the linkages between Te–O chains. Moreover, the values of Poisson's ratio (σ_m) calculated according to Makishima and Machenzie model (see Table 6) were found to be in good agreement with those determined experimentally in Table 5.

Therefore, the behaviors of Poisson's ratio with increasing Nb_2O_5 concentration over the entire glass compositions confirm the increase in cross-link density and consequently the increase in elastic moduli.

Debye temperature (θ_D) plays an important role in solid materials in the determination of elastic moduli and atomic vibrations. θ_D represents the temperature at which all the high-frequency 'lattice' vibrational modes are excited. It is known that Debye temperature depends directly on the mean ultrasound wave velocity [29], so Debye temperature increases as the modifier Nb_2O_5 concentration increases, Table 3. The increase in θ_D can be explained by taking into account two factors. The first is the increase in the uniform distribution of Nb^{5+} ions among the Te–O chains, and consequently the increase in the cross-link density of the glass network structure. The second is the increase in the relative strength of bonds.

Microhardness (H) expresses the stress required to eliminate the free volume of the glass. The free volume in the glass is the openness of the glasses over that of the corresponding crystals [18]. The variation of H with the contents of Nb_2O_5 mol% is tabulated in Table 5. It can be seen that the micro-hardness has the same attitude as the elastic moduli with increase Nb_2O_5 mol% concentration, and hence the observed increase in H is related to the increase in the rigidity of these glasses.

It is of great interest to interpret the variation in the experimental elastic behavior observed in this study with the bulk compression model put forward by Bridge et al. [19] and extended by Abd El-Moneim [30,31] for predicting the compositional dependence of elastic moduli of poly component oxide glasses. Table 6 gives the values of theoretical bond compression bulk modulus (K_{bc}), ratio of (K_{bc}/K_{exp}) and ring diameter (ℓ). It is quite clear from Table 6 that the value of the bond compression bulk modulus (K_{bc}) decreased from for all glass compositions as a direct effect of insertion of Nb_2O_5 modifier mol% content into the glass network. This decrease in K_{bc} is expected since K_{bc} depends on the number of the network bonds per unit volume (n_b) and the average bond lengths.

In general, the ratio (K_{bc}/K_{exp}) is a measure of the extent to which bond bending is governed by the configuration of the network bonds, i.e. this ratio is assumed to be directly proportional to the ring diameter and inversely proportional to the experimentally determined elastic moduli. Therefore, the values of (K_{bc}/K_{exp}) ratio and (ℓ) were found to decrease with addition of Nb_2O_5 modifier mol% content, confirming the increase in elastic. This observation is mainly due to the change in [TeO_4] tbps into [TeO_3] tps which causes the increase in non-bridging oxygen atoms and consequently the decrease in the number of network bonds per unit volume.

4.3. Artificial intelligence technique

In this section, we have designed a model using one of the artificial intelligence techniques (ANN) as a training model in order to be used for prediction of the density, both ultrasonic velocities (longitudinal & shear) and elastic moduli (longitudinal & shear) of our investigated glass series as shown in Table 7. More than 50 glass samples [32–41] were used for the training model. The main advantage of our model is that it enables the direct simulation of very important parameters of glasses such as density, both ultrasonic velocities (longitudinal & shear) and elastic moduli without melting raw material oxides (as in some cases, they are of high costs), depending on some theoretical parameter such as Molecular weight, dissociation energy of oxides as inputs for the model to give the predicted outputs.

Figs. 7–11 show the plots of the experimentally obtained values of density, both ultrasonic velocities (longitudinal & shear), and elastic moduli (longitudinal & shear) against those predicted using our model. The solid straight lines represent slopes which are near to unity implying the good agreement between the experimentally obtained results and those predicted. Considering the uncertainty

Table 7
Measured density (ρ (M)), predicted density (ρ (ANN)), measured longitudinal velocity (U_l (M)), predicted longitudinal velocity (U_l (ANN)), measured shear velocity (U_s (M)), predicted shear velocity (U_s (ANN)), experimental longitudinal modulus (L (M)), predicted longitudinal modulus (L (ANN)), experimental shear modulus (G (M)) and predicted shear modulus (G (ANN)).

TeO_2	WO_3	K_2O	CeO_2	CuO	B_2O_3	Li_2O	Bi_2O_3	V_2O_5	La_2O_3	Nb_2O_5	PbO	Sm_2O_3	BaO	ρ (M)	ρ (ANN)	U_l (M)	U_l (ANN)	U_s (M)	U_s (ANN)	L (M)	L (ANN)	G (M)	G (ANN)
0.8	0.2	0												5.77	5.77	3366	3366	1951	1951	65.35	65.35	21.94	21.94
0.8	0.15	0.05												5.45	5.45	3288	3289	1888	1888	58.94	58.97	19.44	19.44
0.8	0.1	0.1												5.09	5.09	3190	3188	1805	1805	51.82	51.75	16.58	16.59
0.8	0.05	0.15												4.77	4.77	3130	3126	1734	1737	46.68	46.57	14.33	14.37
0.8	0	0.2												4.5	4.5	3058	3062	1681	1678	42.07	42.18	12.71	12.68
0.9			0.1											5.71	5.71	3429	3432	2102	2101	67.1	67.19	25.2	25.18
0.84				0.16										5.62	5.62	3390	3389	1981	1981	64.6	64.55	22.06	22.07
0.821				0.179										5.71	5.71	3476	3470	1887	1890	68.95	68.72	20.32	20.38
0.81				0.19										5.79	5.79	3477	3489	2034	2029	69.93	70.42	23.93	23.81
0.797				0.203										5.61	5.61	3684	3679	2232	2234	76.11	75.92	27.94	27.99
0.1					0.6	0.3								2.58	2.58	5869	5866	3381	3382	88.87	88.78	29.49	29.52
0.2					0.5	0.3								2.92	2.92	5556	5564	3089	3086	90.11	90.38	27.85	27.8
0.3					0.4	0.3								3.18	3.18	5090	5080	2875	2879	82.31	81.99	26.26	26.33
0.35					0.35	0.3								3.4	3.4	4714	4719	2752	2750	75.64	75.82	25.78	25.74
0.5							0	0.5						4	3.99	3655	3655	2096	2096	53.38	53.35	17.55	17.55
0.5							0.05	0.45						4.38	4.38	3591	3593	2056	2056	56.43	56.56	18.5	18.51
0.5							0.1	0.4						4.8	4.79	3507	3504	1995	1995	59	58.77	19.09	19.06
0.5							0.15	0.35						5.19	5.2	3416	3416	1937	1937	60.54	60.66	19.47	19.49
0.5							0.2	0.3						5.62	5.62	3330	3333	1882	1883	62.36	62.41	19.92	19.92
0.5							0.25	0.25						6.03	6.03	3250	3250	1833	1832	63.71	63.7	20.26	20.25
0.65				0				0.35						4	4	3992	3989	2362	2364	63.68	63.57	22.29	22.32
0.65				0.075				0.275						4.38	4.38	3694	3694	2159	2159	59.73	59.73	20.4	20.39
0.65				0.1				0.25						4.8	4.8	3364	3369	1950	1950	54.3	54.45	18.24	18.23
0.65				0.125				0.225						5.19	5.19	3210	3204	1859	1860	53.46	53.27	17.94	17.94
0.65				0.15				0.2						5.62	5.62	3066	3064	1769	1771	52.87	52.8	17.59	17.65
0.65				0.175				0.175						6.03	6.03	2939	2940	1682	1681	52.11	52.14	17.06	17.04
0.9									0.1					5.69	5.69	3415	3419	2093	2091	66.3	66.44	24.9	24.86
0.669										0.124	0.207			5.89	5.89	3294	3296	1906	1906	63.9	63.96	21.4	21.39
0.75									0.04		0.21			6.15	6.14	3038	3034	1711	1713	56.7	56.58	18	18.03
0.9												0.1		5.78	5.78	3447	3441	2149	2152	68.7	68.46	26.7	26.77
1														5.1	5.1	3404	3413	2010	2005	59.1	59.44	20.6	20.52
0.85	0.15													5.25	5.25	3532	3529	2031	2032	65.5	65.39	21.66	21.69
0.8	0.2													5.77	5.77	3366	3366	1951	1950	65.35	65.34	21.94	21.93
0.79	0.21													5.39	5.39	3561	3559	2080	2081	68.35	68.25	23.32	23.35
0.67	0.33													5.7	5.7	3555	3557	2098	2097	72.04	72.11	25.09	25.07
0.77	0.14												0.09	5.67	5.67	3378	3380	1952	1951	64.7	64.77	21.6	21.58
0.74	0.21		0.05											5.78	5.78	3408	3411	2011	2010	67.14	67.25	23.38	23.35
0.77	0.2								0.03					6.03	6.03	3480	3480	2035	2035	73	72.98	24.96	24.97
0.5	0.3										0.2			6.68	6.68	3169	3168	1786	1786	67.1	67.06	21.3	21.31
0.75	0.2											0.05		6.11	6.11	3515	3514	2067	2067	75.49	75.45	26.1	26.11
0.95										0.05				5.48	5.75	3352	3320	1876	1863	61.52	63.39	19.27	19.95
0.9										0.1				5.41	5.86	3464	3421	1911	1898	64.96	68.57	19.77	21.1
0.85										0.15				5.3	5.54	3677	3647	1949	1936	71.68	73.74	20.14	20.79
0.8										0.2				5.24	5.12	3922	3898	2087	2080	80.63	77.74	22.83	22.14
0.9											0.1			5.85	5.96	3091	3068	1746	1733	55.84	56.1	17.82	17.91
0.7										0.2	0.1			5.53	5.32	3767	3752	2079	2070	78.46	74.84	23.9	22.78
0.8											0.2			5.9	5.24	3692	3701	2177	2186	80.48	71.73	27.98	25.03
0.7										0.1	0.2			6.03	6.23	3151	3144	1784	1774	59.82	61.59	19.18	19.59
0.6										0.2	0.2			7.28	7.57	2882	2890	1495	1486	60.45	63.17	16.27	16.7
0.75							0.05			0.2				5.33	5.85	3633	3605	1879	1889	70.35	76.04	18.82	20.89
0.7							0.05			0.25				5.13	4.95	3990	4007	2175	2192	81.67	79.45	24.27	23.78

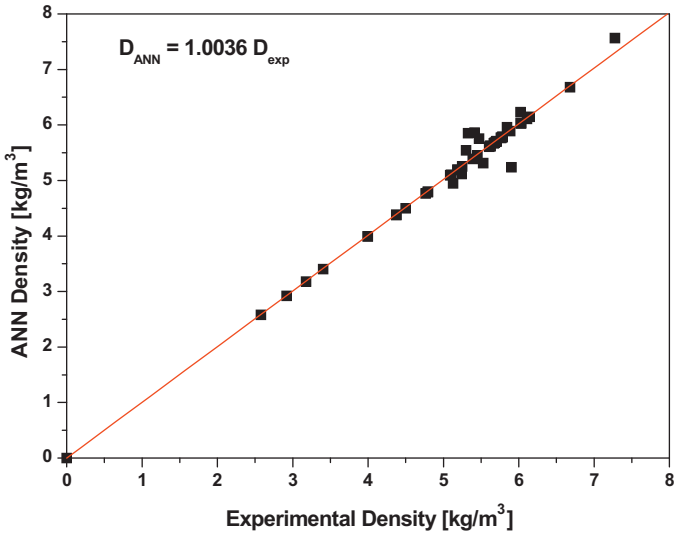

Fig. 7. Plot of the experimentally measured density of some tellurite glasses and predicted density using (ANN).

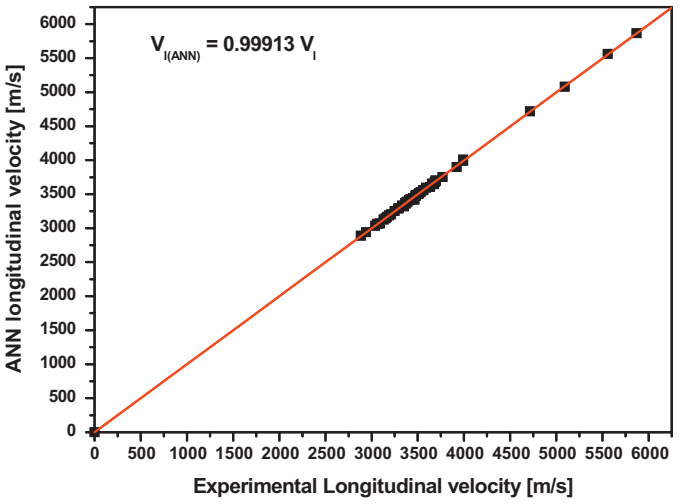

Fig. 8. Plot of the experimentally measured longitudinal velocity (V_l) of some tellurite glasses and predicted ($V_{l(\mathrm{ANN})}$) using (ANN).

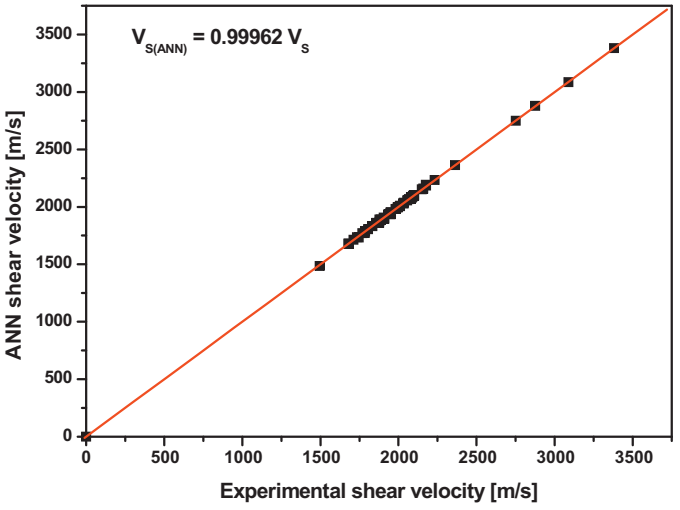

Fig. 9. Plot of the experimentally measured shear velocity (V_S) of some tellurite glasses and predicted ($V_{S(\mathrm{ANN})}$) using (ANN).

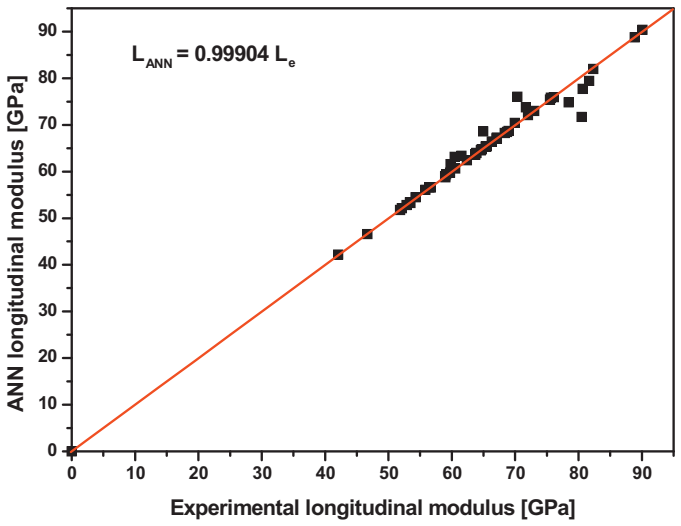

Fig. 10. Plot of the experimentally measured longitudinal modulus (L_e) of some tellurite glasses and predicted (L_{ANN}) using (ANN).

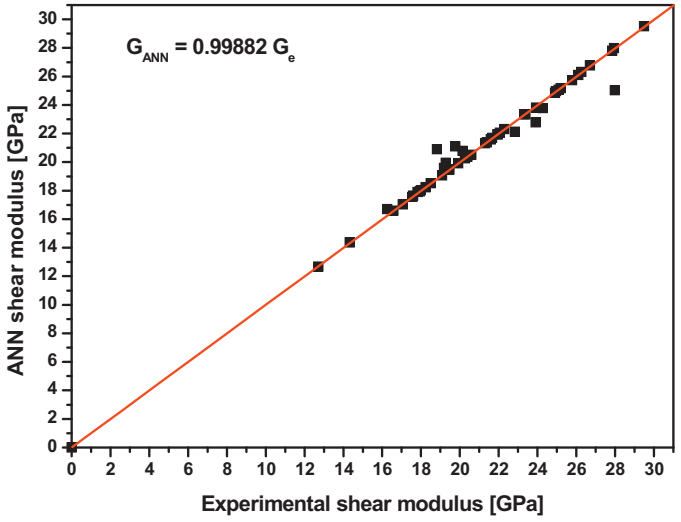

Fig. 11. Plot of the experimentally measured shear modulus (G_e) of some tellurite glasses and predicted (G_{ANN}) using (ANN).

of experimental data, the agreements in Figs. 7–11 are considered to be very satisfactory. It shows that the model we designed gives a better agreement as compared with Makishima and Machenzie model. The difference between the predicted and experimentally obtained values is lower than 0.5% in most cases and never greater than 5% in the investigated glasses. Such a good approach for predicting our results reveals that our model is valid.

5. Conclusions

An artificial intelligence model have been developed for direct estimation of the density, both ultrasonic velocities (longitudinal & shear) and elastic moduli of oxide glasses from their compositions. Excellent agreements between the measured values and the predicted values were obtained for over 50 different tellurite glass compositions. Using this model we have successfully prepared a new 4 glass series in $x\mathrm{Nb_2O_5}$–$(1-x)\mathrm{TeO_2}$, $0.1\mathrm{PbO}$–$x\mathrm{Nb_2O_5}$–$(0.9-x)\mathrm{TeO_2}$, $0.2\mathrm{PbO}$–$x\mathrm{Nb_2O_5}$–$(0.8-x)\mathrm{TeO_2}$ and $0.05\mathrm{Bi_2O_3}$–$x\mathrm{Nb_2O_5}$–$(0.95-x)\mathrm{TeO_2}$. Such a model presents a new possibility for the investigation of glass structures before making experimental works. The experimental results of ultrasonic veloc-

ities and elastic moduli for these 4 glass series showed that the Nb_2O_5 acted as a network modifier which provides oxygen ions to change [TeO_4] tbps into [TeO_3] tps.

References

[1] T. Sekiya, N. Mochida, A. Ohtsuka, J. Non-Cryst. Solids 144 (1992) 128.
[2] M. Tatsumisago, T. Minami, Y. Kowada, Phys. Chem. Glasses 35 (1994) 89.
[3] B. Chowdari, P. Kumari, J. Non-Cryst. Solids 197 (1996) 31.
[4] A. Pan, A. Ghosh, Phys. Rev. B 60 (1999) 3224.
[5] H. Sakata, K. Sega, B. Chaudhuri, Phys. Rev. B 60 (1999) 3230.
[6] A. Jha, S. Shen, M. Naftaly, Phys. Rev. B 62 (2000) 6215.
[7] N.B. Mohamed, A.K. Yahya, M.S.M. Deni, S.N. Mohamed, M.K. Halimah, H.A.A. Sidek, J. Non-Cryst. Solids 356 (2010) 1626.
[8] Y. Wang, S. Dai, F. Chen, T. Xu, Q. Nie, Mater. Chem. Phys. 113 (2009) 407.
[9] A. Chagraoui, A. Tairi, K. Ajebli, H. Bensaid, A. Moussaoui, J Alloys Compd. 495 (2010) 67.
[10] X. Zou, H. Toratani, J. Non-Cryst. Solids 290 (2001) 180.
[11] K.A. Kheireldin, Proc. of the 3rd Int. Conference Hydroinformatics, Copenhagen–Denmark, (1998), 1998.
[12] M.A.M. Abdeen, Scientific Journal Faculty of Engineering-Alexandria University, Egypt 40 (4) (2001) 539.
[13] B.S.M. Allam, Ph.D., Thesis, Faculty of Engineering, Cairo University, Egypt, 2005.
[14] M.A.M. Abdeen, J. Mech. Sci. Technol., KSME Int. J., Korea 20 (2006) 1691.
[15] M.A.M Mohamed, M. Sc., Thesis, Faculty of Engineering, Cairo University, Egypt, 2006.
[16] M.A.M. Abdeen, J. Mech. Sci. Technol., KSME Int. J., Korea 22 (2008) 1830.
[17] M.A.M. Abdeen, H. Hodhod, Sci. Res. Org. Eng. 2 (6) (2010) 408.
[18] A.K. Varshneya, Fundamentals of Inorganic Glasses, Academic Press, New York, 1994.
[19] B. Bridge, N.D. Patel, D.N. Waters, Phys. Stat. Sol. (a) 77 (1983) 655.
[20] B. Bridge, A.A. Higazy, Phys. Chem. Glasses 27 (1986) 1.
[21] A. Makishima, J.D. Mackenzie, J. Non-Cryst. Solids 12 (1973) 35.
[22] A. Makishima, J.D. Mackenzie, J. Non-Cryst. Solids 17 (1975) 147.
[23] Y. Shin, Neuralyst™ User's Guide, Cheshire Engineering Corporation Publisher (1994).
[24] D.R. Lid, CRC Handbook of Chemistry and Physics, 80th edition, CRC Press, London, 2000.
[25] T. Komatsu, H. Tawarayama, H. Mohri, K. Matusita, J. Non-Cryst. Solids 135 (1991) 105.
[26] J. Lin, W. Huang, L. Ma, Q. Bian, S. Qin, H. Wei, J. Chen, Mater. Sci. Poland 27 (2009) 329.
[27] J. Galy, O. Lindqvist, J. Solid State Chem. 27 (1979) 279.
[28] S. Blanchandin, J.C. Champarnaud-Mesjard, P. Thomas, J. Alloys Compd. 306 (2000) 175.
[29] O.L. Anderson, in: W.P. Mason (Ed.), Physical Acoustics, vol. B45, no. (III), Academic Press, New York, 1965.
[30] A. Abd El-Moneim, Phys. B: Condens. Matter. 325 (2003) 319.
[31] A. Abd El-Moneim, L. Abd El-Latif, Phys. Chem. Glasses 44 (6) (2003) 446.
[32] M.A. Sidkey, M.S. Gaafar, Phys. B: Condens. Matter 348 (2004) 46.
[33] R. EL-Mallawany, J. Mater. Res. 5 (1990) 2218.
[34] A. Paul, P. Roychoudhury, S. Mukherjee, C. Basu, J. Non-Cryst. Solids 275 (2000) 83.
[35] E.F. Lambson, G.A. Saunders, S. Hart, J. Mater. Sci. Lett. 4 (1985) 669.
[36] R. EL-Mallawany, G.A. Saunders, J. Mater. Sci. Lett. 7 (1988) 870.
[37] R. EL-Mallawany, G.A. Saunders, J. Mater. Sci. Lett. 6 (1987) 443.
[38] S. Hart, J. Mater. Sci. 18 (1983) 1264.
[39] V. Rajendran, N. Palanivelu, B.K. Chaudhuri, K. Goswami, J. Non-Cryst. Solids 320 (2003) 195.
[40] Y.B. Saddeek, H.A. Afifi, N.S. Abd El-Aal, Phys. B: Condens. Matter 398 (2007) 1.
[41] N.S. Abd El-Aal, H.A. Afifi, Arch. Acoustics 34 (2009) 641.